ADVANCED MATERIALS
www.advmat.de

Amine-Based Polar Solvent Treatment for Highly Efficient Inverted Polymer Solar Cells

*Bo Ram Lee, Eui Dae Jung, Yun Seok Nam, Minbok Jung, Ji Sun Park, Seungjin Lee, Hyosung Choi, Seo-Jin Ko, Na Ra Shin, Young-Kuk Kim, Sang Ouk Kim, Jin Young Kim, Hyung-Joon Shin, Shinuk Cho, and Myoung Hoon Song**

Bulk heterojunction (BHJ) polymer solar cells (PSCs) are promising devices for an alternative energy source because of their low cost, large area, and easy solution-based fabrication with mechanical flexibility.[1–7] Moreover, extensive efforts have been made to enhance their power conversion efficiency (PCE) by the use of low-bandgap donor materials[8–11] for a broader absorption range of the solar spectrum and device optimization.[12–17]

A corrosive hole-transporting layer such as poly(3,4-ethylen edioxylenethiophene):poly(styrenesulfonic acid) (PEDOT:PSS) and a low work function (WF) metal cathode such as Ca, Ba, or Al are usually used in conventional PSCs, which require strict encapsulation to prevent degradation under oxygen and moisture for long-term device stability.[18–20] Meanwhile, inverted structure PSCs (iPSCs) show much better air-stability using metal oxides (ZnO, TiO_x, etc.) as buffer layers and high WF metals (Ag or Au) as top electrodes.[7,21–23] Furthermore, a favorable vertical phase separation and concentration gradient in the active layer can be expected in the iPSC configuration.[24,25]

In spite of the many advantages of iPSCs, device performance given in terms of short circuit current (J_{sc}), fill factor (*FF*), and PCE is not very high owing to the large contact barrier between the active layer and the electrodes. A Au anode with a p-type MoO_3 (hole-extracting) layer deposited on it[26] has been used as an ohmic contact to the highest occupied molecular orbital (HOMO) level of the active layer and enables abundant hole extraction at the anode in iPSCs. However, the contact barrier between the transparent cathode, including n-type metal oxides, and the lowest unoccupied molecular orbital (LUMO) of the acceptor of an active layer still exists in iPSCs, leading to inefficient charge transport and extraction.[14,27,28] In this regard, bandgap engineering at the interface between inorganic electrodes and organic semiconductors is central to current research interests.[27] One way to solve the problem of this large energy barrier turned out to be by incorporating an interfacial dipole layer or surface modifier, such as a self-assembled dipole monolayer (SADM),[27] ionic liquid molecules (ILMs),[28] a conjugated polyelectrolyte (CPE),[14,29] an alcohol/water-soluble conjugated polymer,[7,13,15,30,31] or a polar solvent.[32,33] The energy barrier between the cathode and an active layer can be controlled by these interfacial dipole layers, leading to improved electron transport and extraction. Moreover, it can minimize interfacial contact resistance and prevent undesired charge recombination, which can result in enhanced device efficiency.

In this Communication, we report remarkable enhancement of iPSC efficiency by the reduction of the energy barrier between the conduction band (CB) of ZnO and the LUMO of the acceptor in an active layer, using a simple and effective method of polar solvent treatment on the ZnO layer, specifically, with 2-methoxyethanol (2-ME) and ethanolamine (EA) co-solvents. The dipolar polarization, which arises spontaneously from the absorption of EA end groups such as amine (NH_3) and hydroxyl (OH) groups on ripple-structure zinc oxide (ZnO-R), lowers the contact barrier for the electron transport and extraction and leads to enhanced electron mobility, suppression of bimolecular recombination, reduction of the contact resistance and series resistance (R_s), and remarkable enhancement of PCE from 6.71% to 8.69%.

Figures 1a and b illustrate the device architecture of our iPSCs and the chemical structures of thieno[3,4-b]thiophene/benzodithiophene (PTB7, 1-material Inc.), [6,6]-phenyl-C_{71}-butyric

B. R. Lee, E. D. Jung, Y. S. Nam, M. Jung, S. Lee, N. R. Shin, Prof. H.-J. Shin, Prof. M. H. Song
School of Mechanical and Advanced Materials Engineering
KIST-UNIST Ulsan Center for Convergent Materials
Low Dimensional Carbon Materials Center
Ulsan National Institute of Science and Technology (UNIST)
UNIST-gil 50, Ulsan, 689–798, Republic of Korea
E-mail: mhsong@unist.ac.kr
Dr. J. S. Park
Energy Nanomaterials Research Center
Korea Electronics Technology Institute (KETI)
68 Yatap-dong, Bundang-gu, Seongnam-si
Gyeonggi-do, 463–816, Republic of Korea
H. Choi, S.-J. Ko, Prof. J. Y. Kim
Interdisciplinary School of Green Energy and KIER-UNIST Advanced Center for Energy
Ulsan National Institute of Science and Technology (UNIST)
UNIST-gil 50, Ulsan, 689–798, Republic of Korea
Dr. Y.-K. Kim
Korea Institute of Materials Science (KIMS)
#797 Changwondaero, Changwon, Kyungnam, 641–010
Republic of Korea
Prof. S. O. Kim
Center for Nanomaterials and Chemical Reactions
Institute for Basic Science (IBS)
Department of Materials Science & Engineering
Korea Advanced Institute of Science and Technology (KAIST)
Daejeon, 305–701, Republic of Korea
Prof. S. Cho
Department of Physics and EHSRC
University of Ulsan
Ulsan, 680–749, Republic of Korea

DOI: 10.1002/adma.201302991

© 2013 WILEY-VCH Verlag GmbH & Co. KGaA, Weinheim

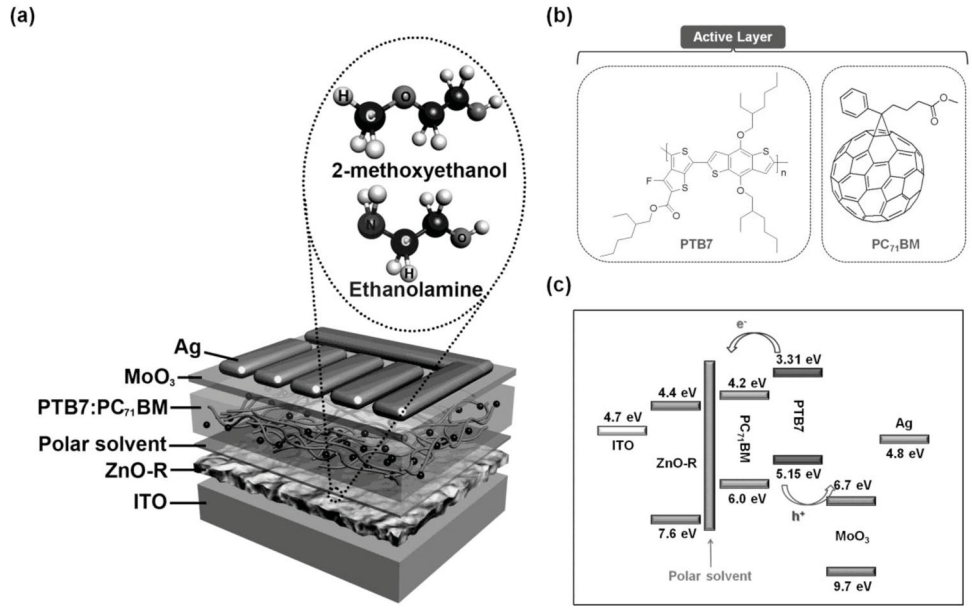

Figure 1. The iPSCs based on PTB7:$PC_{71}BM$ blend with polar solvent. a) Device architecture of the iPSCs. Inset: The chemical structures of the interfacial layer with EA and 2-ME. b) The chemical structures of the active materials. The donor material is PTB7 and the acceptor material is $PC_{71}BM$. c) Schematic energy diagrams for flat band conditions of iPSCs.

acid methyl ester ($PC_{71}BM$), 2-ME, and EA used in this work. The devices consist of indium tin oxide (ITO) as a transparent cathode, ZnO-R as an electron extraction layer, a polar solvent as a surface modifier, an active layer with PTB7 as the donor material and $PC_{71}BM$ as the acceptor material, MoO_3 as a hole extraction layer, and Ag as an anode. A 30 nm thick n-type ZnO-R layer was prepared on ITO by a slow heating process, resulting in a denser film with higher surface area than a ZnO planar film. A denser ZnO-R film has fewer defects, leading to lower leakage current, larger shunt resistance, and higher *FF* in comparison with a ZnO planar film.[34] Next, UV-ozone treatment was conducted on the ZnO-R to avoid electron trapping, which led to improved charge transport and collection.[17] For the interfacial modification of the top surface of the ZnO-R layer, various polar solvents were spin-coated at 3000 rpm onto a ZnO-R layer and then annealed at 110 °C for 10 min to remove residual solvent. More details of the preparation of the ZnO-R layer and surface modification of the ZnO-R layer using polar solvents are given in the Experimental Section. The PTB7 (10 mg):$PC_{71}BM$ (15 mg) blend solution was dissolved in a mixed solvent of chlorobenzene/1,8-diiodoctane (97:3% by volume), and the solution (concentration, 25 mg mL^{-1}) was spin-cast at 800 rpm on top of the buffer layer to give a 80 nm thick active layer. A 5 nm thick MoO_3 layer and a 100 nm thick Ag layer were thermally evaporated onto the active layer at a slow deposition rate of 0.03 nm s^{-1}.

Figure 1c shows the energy level diagram of the fabricated iPSCs. For higher efficiency of our iPSCs, well-matched work functions between the CB of ZnO-R and LUMO of $PC_{71}BM$ and also the suppression of bimolecular recombination are required.

Device characterizations of the iPSCs with and without treatment by polar solvents such as methanol, ethanol, 2-ME, and 2-ME+EA on top of the ZnO-R are presented in terms of current density versus voltage (*J*–*V*) under 1000 W m^{-2} air mass 1.5 global (AM 1.5G) illumination in **Figure 2**a. The reference iPSCs without polar solvent treatment (reference device) exhibited J_{SC} = 13.70 mA cm^{-2}, open circuit voltage (V_{OC}) of 0.71 V, *FF* = 0.69, and PCE (η) = 6.71%. On the other hand, the iPSCs with polar solvent treatment showed remarkably enhanced device efficiency in comparison with the reference device. Among iPSCs with polar solvent treatment, optimized iPSCs using 2-ME+EA (1% by volume) co-solvents as a surface modifier of the ZnO-R layer exhibited the best device performance. The detailed device characteristics with and without various polar solvent treatments are summarized in **Table 1**. Moreover, the iPSCs with 2-ME and EA co-solvent treatment were optimized through different concentration of co-solvents and the optimized iPSCs with 2-ME+EA (1%) co-solvent treatment showed the highest device performance, with J_{SC} = 16.76 mA cm^{-2}, *FF* = 0.73, and PCE = 8.69%, whereas V_{OC} was similar, at 0.71 V. The use of excessive volume percentage of EA in 2-ME degraded the device performance because higher interfacial negative dipoles, which reduced the contact barrier between ZnO and active layers, were not formed and the extraction of electrons was more difficult toward the cathode in a thicker EA interfacial insulator (Fig. S1 and Table S1 in the Supporting Information).[28,35,36] The shift of the vacuum level of ZnO-R by the interfacial dipole of EA does not affect the V_{OC} value in this study. The external quantum efficiency (EQE) spectra of iPSCs with and without the polar solvent treatment on top of the ZnO-R are shown in Figure 2b. The iPSCs with polar solvent treatment exhibited higher values, from 350 to 700 nm, than that without polar solvent treatment. The iPSCs with 2-ME+EA co-solvents as a surface modifier of the ZnO-R layer showed the highest EQE value with a maximum value of 75% at 630 nm.

© 2013 WILEY-VCH Verlag GmbH & Co. KGaA, Weinheim
Adv. Mater. **2013**,
DOI: 10.1002/adma.201302991

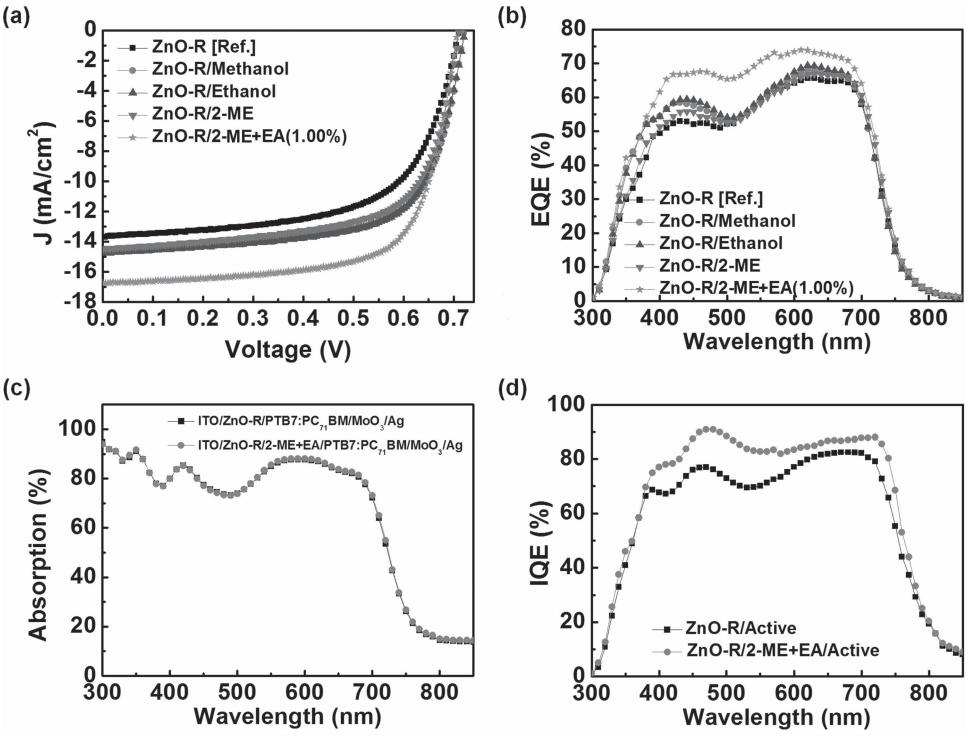

Figure 2. Enhanced device performance in iPSCs with polar solvent treatment. *J–V* characteristics (a) and EQE characteristic (b) under 1000 W m^{-2} AM 1.5G illumination for the reference (black squares), with methanol (gray circles), with ethanol (black triangles), with 2-ME (gray triangles), and with 2-ME+EA (gray stars). Absorption spectra (c) and IQE (d) of the full devices without (ITO/ZnO-R/PTB7:$PC_{71}BM$/MoO_3/Ag; black symbols) and with 2-ME+EA co-solvent treatment (ITO/ZnO-R/2-ME+EA/ PTB7:$PC_{71}BM$/MoO_3/Ag; gray symbols) on a ZnO-R layer.

The internal quantum efficiency (IQE) of iPSCs with and without 2-ME+EA co-solvent treatment, obtained from the absorption spectra (Figure 2c), is shown in Figure 2d. Moreover, the total absorption spectra of iPSCs with and without 2-ME+EA co-solvent treatment were obtained from the reflectance spectra (Fig. S2, Supporting Information), and these two absorption spectra are almost identical regardless of 2-ME+EA co-solvent treatment on ZnO-R. It proves that the 2-ME+EA interfacial treatment on the ZnO-R layer does not affect the absorption of iPSCs. The IQE spectrum of the iPSC with 2-ME+EA interfacial treatment on the ZnO-R layer shows a higher value, above 90%, than that without the 2-ME+EA interfacial layer, which shows around 80% from 400 to 700 nm, as presented in Figure 2d. The wide and high IQE data indicate that the morphology of the blend film is close to the ideal donor and acceptor nanometer-scale morphology and the charge extraction in the active layer and two metal oxide interfaces is all very close to 100% in iPSCs with 2-ME+EA co-solvent treatment on ZnO-R.

Table 1. Summarized device performances of iPSCs with and without polar solvent treatment, measured under 1000 W m^{-2} AM 1.5G illumination.

Device configuration	J_{sc} [mA cm^{-2}]	V_{oc} [V]	*FF*	η [%]	R_s [Ω cm^2]
ITO / ZnO-R / PTB7:$PC_{71}BM$ / MoO_3 / Ag	13.70	0.71	0.69	6.71	1.08
ITO / ZnO-R / methanol / PTB7: $PC_{71}BM$ / MoO_3 / Ag	14.69	0.72	0.73	7.72	0.73
ITO / ZnO-R / ethanol / PTB7: $PC_{71}BM$ / MoO_3 / Ag	14.75	0.72	0.72	7.65	0.95
ITO / ZnO-R / 2-ME / PTB7: $PC_{71}BM$ / MoO_3 / Ag	14.45	0.71	0.71	7.28	0.90
ITO / ZnO-R / 2-ME+EA(1%) / PTB7: $PC_{71}BM$ / MoO_3 / Ag	16.76	0.71	0.73	8.69	0.69

The remarkable device performance following 2-ME+EA treatment on ZnO-R originates from the spontaneous dipolar polarization. The energy band diagrams for ZnO-R/active layer junctions with and without 2-ME+EA co-solvent treatment are illustrated in **Figure 3**a. For higher device efficiency, the CB of the ZnO-R should match well with the LUMO of $PC_{71}BM$. After spin-casting of the 2-ME+EA co-solvent on top of ZnO-R, the CB of the ZnO-R was reduced from 4.4 eV to 3.9 eV, as confirmed by ultraviolet photoelectron spectroscopy (UPS) measurements, as shown in Figure 3b. There is no considerable difference in topography between ZnO-R and 2-ME+EA/ZnO-R surfaces (**Figure 4**a), however, we can also confirm the change of surface potential after 2-ME+EA treatment by means of scanning Kelvin probe microscopy (SKPM). We measured the contact potential difference (V_{CPD}) between the tip and the partially 2-ME+EA-covered ZnO-R surface (Figure 4b). SKPM measurement revealed an increase of surface potential of around 82.6 meV on the active layer (Figure 4c). From UPS and SKPM results, we can understand that the 2-ME+EA active layer plays an important role in enhanced device performance. Thus, the

© 2013 WILEY-VCH Verlag GmbH & Co. KGaA, Weinheim

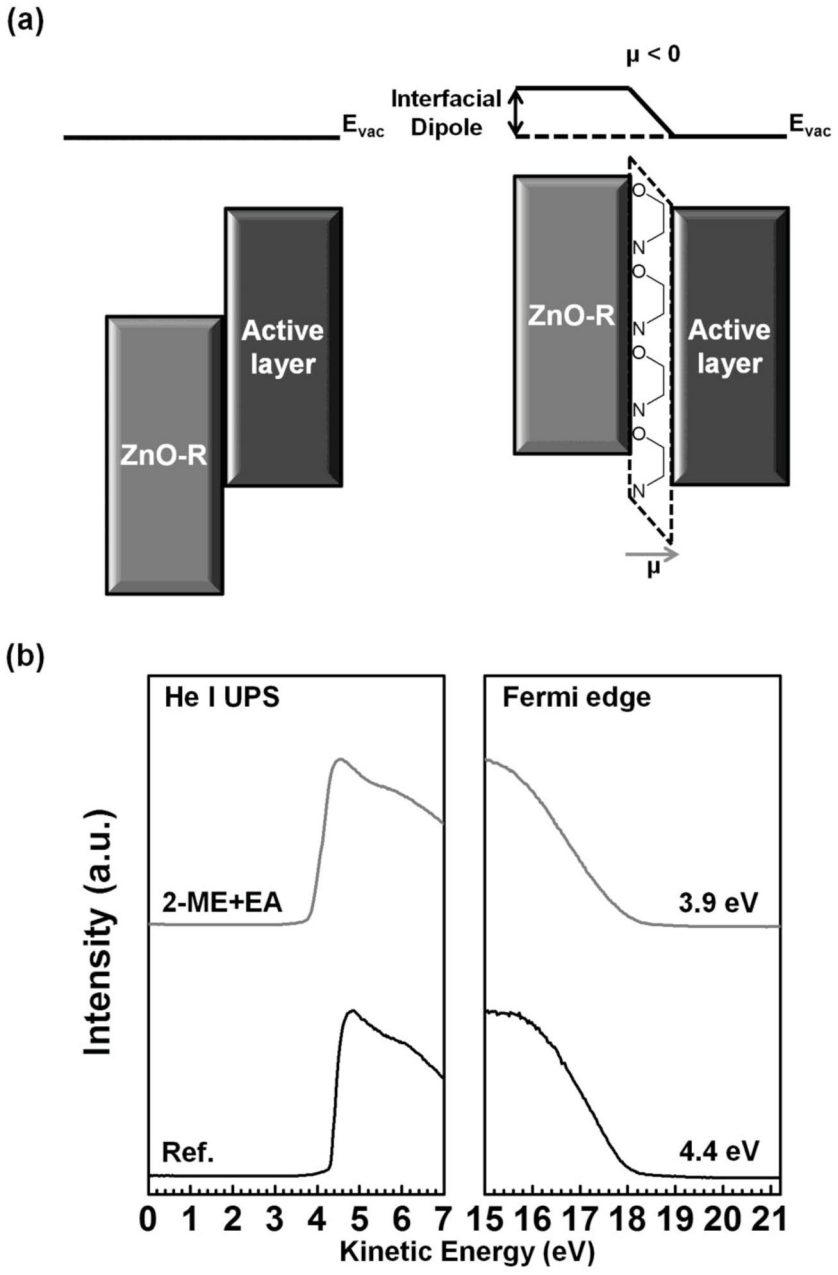

Figure 3. Schematic energy level diagrams. a) Schematic energy diagrams for flat band conditions at the ZnO-R/active layer without (left) and with (right) 2-ME+EA co-solvent treatment on the ZnO-R layer. b) UPS measurement of ZnO-R (black line) and ZnO-R with (gray line) 2-ME+EA co-solvent treatment.

interfacial modification of the EA on the ZnO-R layer creates an ohmic contact through changes of the energy barrier between the ZnO-R and active layer. This ideal ohmic contact provides promoted overall electron transport and high-electron-mobility pathways (see Fig. S3, Supporting Information).

The interfacial dipolar polarization, which arises from the absorption of EA end groups, such as amine and hydroxyl groups, on ZnO-R was confirmed by X-ray photoelectron spectroscopy (XPS) and contact angle measurement. To confirm the adsorption of functional groups of EA on ZnO-R, ethylene diamine (EDA, $NH_2CH_2CH_2NH_2$) with 2-ME was coated on ZnO-R as a reference because EDA is a well-known bidentate ligand and two nitrogen atoms of EDA bond to a Zn metal using electron pairs. Therefore, a uniform EDA layer was readily formed on the ZnO-R surface through a chemical bond between two nitrogen atoms of EDA and the Zn metal of ZnO-R. While nitrogen atoms with higher electronegativity existed near the ZnO-R surface, aliphatic groups ($–CH_2CH_2–$) with lower electronegativity existed oriented upward in the monolayer. Therefore, the contact angle increased with concentration of EDA in 2-ME until two nitrogen atoms of EDA covered all the Zn metal in the ZnO surface (3.33 vol% of EDA in 2-ME, maximum contact angle 65.0°), and then decreased as the concentration of EDA in 2-ME was further increased because the absorption of EDA end groups on the ZnO competed with each other for the excess EDA molecules and some of the hydrophilic end groups of EDA oriented upward (see Fig. S4, Supporting Information). The result of contact angle measurement with EA molecules on ZnO-R also showed the same trend as with EDA molecules. The amine and hydroxyl end groups of EA were absorbed on the ZnO-R surface and hydrophobic ethylene groups existed oriented upward because the interaction between ZnO and hydroxyl groups could also be hydrogen bonding between oxygen atom in ZnO and hydrogen atom in hydroxyl groups, as represented in Figure 3a. The contact angle was maximized as 37.9° at the specific concentration of EA (1%) in 2-ME where the efficiency of iPSC also showed the highest value of 8.69% (Fig. S1, Supporting Information), and then decreased with excess EA. These results indicate that the EA molecules with moderate concentration in 2-ME create the negative dipoles, and they lead to reduction of the contact barrier after surface treatment of EA on ZnO-R. The adsorption of amine groups of EA on Zn metals of ZnO-R and the existence of EA molecules on ZnO-R were also confirmed using XPS measurement by tracking the position and shape of the N 1s peak at 400.1 eV (N–C peak) and 398.8 eV (N–Zn peak) (Fig. S5, Supporting Information).[37–39]

The effect of interfacial dipolar polarization on electron transport efficiency could be confirmed by the electron-only device characteristics. Electron-only device configurations of ITO/ZnO-R/PTB7:PC_{71}BM/LiF/Al with and without 2-ME+EA co-solvent treatment were prepared and the electron mobility was obtained from the Mott–Gurney space-charge-limited current (SCLC) equation:

© 2013 WILEY-VCH Verlag GmbH & Co. KGaA, Weinheim
Adv. Mater. **2013**,
DOI: 10.1002/adma.201302991

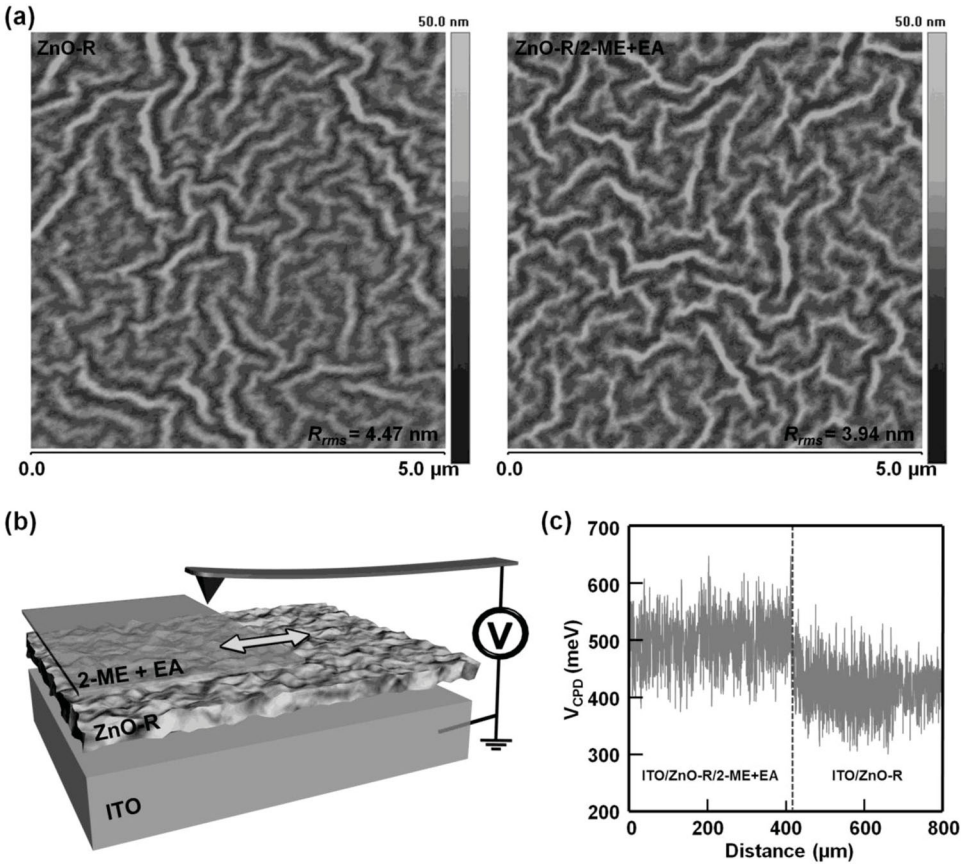

Figure 4. Surface characteristic for ZnO-R with and without 2-ME+EA co-solvent treatment. a) The surface property and morphology of the ZnO-R films without (left) and with (right) the 2-ME+EA layer were characterized by AFM. The AFM images (5 μm × 5 μm area) were obtained using the tapping mode. The measured rms roughness of the ZnO-R layer with and without co-solvent treatment is 3.94 and 4.47 nm, respectively. b) Schematic illustration of the experimental setup for SKPM. c) V_{CPD} as a function of position measured by SKPM.

$$J = \frac{9}{8}\mu_{eff}\varepsilon_0\varepsilon_r\frac{V^2}{d^3} \quad (1)$$

where J is the current density, μ_{eff} the effective charge carrier mobility, which includes the effect of transport efficiency or traps, ε_0 the permittivity of free space, ε_r the relative permittivity of the medium, V the applied voltage, and d the thickness of the active layer. The J–V characteristics of electron-only devices were fitted with the SCLC model as given in Equation (1) (see Fig. S3, Supporting Information). According to the relative dielectric constant (3.4)[30] and the measured thickness of 80 nm for the active layer, the effective electron mobility (μ_{eff}) was calculated to be 5.44×10^{-6} cm^2 V^{-1} s^{-1} for the device without co-solvent treatment. In contrast, the device with co-solvent treatment showed the higher effective mobility of 5.75×10^{-4} cm^2 V^{-1} s^{-1}, which corresponds to an approximately hundredfold increase compared to the device without co-solvent treatment. This result along with UPS and SKPM measurements indicates that the polar co-solvent treatment on the ZnO-R layer effectively promoted electron transport and extraction.

The ZnO-R surface with 2-ME+EA co-solvent treatment was significantly smoother than that without 2-ME+EA co-solvent treatment as confirmed by atomic force microscopy (AFM) in Figure 4a. The measured root-mean-square (rms) roughness of the ZnO-R layer with and without co-solvent treatment is 3.94 and 4.47 nm, respectively. Furthermore, the 2-ME+EA treatment on ZnO-R minimizes the contact resistance between the ZnO-R and active layer due to the improved compatibility in interface, as confirmed by electrical impedance spectroscopy, as shown in Fig. S6 (Supporting Information). Upon deposition of the 2-ME+EA interfacial layer, the series resistance (R_S) of the device decreased from 1.08 Ω cm^2 to 0.69 Ω cm^2. The combined results, such as higher J_{sc}, *FF*, PCE, and electron mobility and lower resistance, provide clear evidence for the enhanced performance.

To confirm the suppression of the bimolecular recombination by the EA interfacial layer the J–V characterizations of iPSCs with and without 2-ME+EA co-solvent treatment on top of the ZnO-R were measured in the dark, as shown in Fig. S7 (Supporting Information). The dark current density of the iPSCs with 2-ME+EA co-solvent treatment under reverse bias is much smaller than that of the iPSCs without co-solvent treatment, and this lower dark current density, observed from the iPSCs with 2-ME+EA co-solvent treatment, indicates the suppression of the bimolecular recombination by the EA interfacial layer.[31] Thus charge extraction is enhanced.

© 2013 WILEY-VCH Verlag GmbH & Co. KGaA, Weinheim

In addition, the air stability of iPSCs with and without 2-ME+EA co-solvent treatment on ZnO-R layer was measured as a function of storage time under ambient air conditions without any particular device encapsulation, as shown in Fig. S8 (Supporting Information). The PCEs of iPSCs with and without 2-ME+EA co-solvent treatment remained at approximately 60% of the original values even after storage in air for 720 h (30 days), and the slopes of decrease for J_{sc}, *FF*, and PCE values of the iPSCs with and without 2-ME+EA treatment are almost identical. This result indicates that the interaction between the ZnO-R surface and EA is consistent for a long time.

In summary, we have successfully demonstrated highly efficient iPSCs using a simple surface treatment using a polar solvent, which tunes the barrier between the LUMO of the ZnO-R and active layer, and results in improved device performance. In particular, the optimized iPSCs with the 2-ME+EA interfacial layer demonstrated an enhanced J_{sc} of 22%, *FF* of 6%, PCE of 30%, and IQE of 19% compared with iPSCs without that interfacial layer. The high efficiency of the iPSCs originates from interfacial dipolar polarization, which comes spontaneously from the absorption of EA end groups such as amine and hydroxyl groups on ZnO-R. The EA interfacial dipole layer including amine groups creates an ohmic contact, leading to improved electron mobility, suppresses bimolecular recombination, and reduces the contact resistance and series resistance (R_s). This charge-selective interfacial engineering provides a promising method for organic-semiconductor-based devices, such as organic photovoltaics, organic light-emitting diodes (OLEDs), organic thin film transistors, and organic laser diodes.

Experimental Section

ZnO-R/2-ME+EA film fabrication: 0.50 M ZnO-R solutions were prepared by dissolving zinc acetate dehydrate [$Zn(CH_3COO)_2{\cdot}2H_2O$] in 2-ME solution containing EA as a stabilizer and ZnO nanoparticles. This solution was stirred at 60 °C for 30 min to yield a clear and homogeneous solution.[34,40,41] The ZnO-R precursor solution was spin-cast on cleaned ITO substrates after a UV-ozone treatment for 30 min and heated to 380 °C with a heating rate of 20 °C min^{-1}. Subsequently, EA/2-ME was spin-cast at 3000 rpm on top of the ZnO-R layer and then dried at 110 °C for 10 min.

AFM characterization: The surface property and morphology of the ZnO-R films with and without the 2-ME+EA layer were characterized by AFM. The AFM images (5 μm × 5 μm area) were obtained using a Veeco atomic force microscope in tapping mode.

Scanning Kelvin probe microscopy (SKPM) characterization: The surface potential of the active layer and ZnO-R surfaces was measured by SKPM (XE-70, Park Systems, Suwon, Korea). The Pt/Cr-coated conducting tip was modulated by applying AC modulation of 350 mV (rms) at a frequency of 17.5 kHz using a lock-in amplifier (SR-830, Stanford Research Systems, Sunnyvale, CA). The V_{CPD} was obtained by applying a DC feedback voltage to the sample to cancel the electrostatic force component between tip and sample, which is proportional to the first harmonic signal of the lock-in amplifier.

X-ray photoelectron spectroscopy (XPS) characterization: To measure the elemental composition, empirical formula, and chemical state of intrinsic impurities existing in the ZnO-R films with and without 2-ME+EA, XPS investigations were carried out on a Thermo Scientific K-Alpha spectrometer (Thermo Fisher) using Al Kα non-monochromatic X-ray excitation at a power of 72 W, with an analysis area 400 μm in diameter and a pass energy of 50 eV for electron analysis.[42]

Solar cell fabrication: The iPSC devices were fabricated using poly[[4,8-bis[(2-ethylhexyl)oxy]benzo[1,2-b:4,5-b′]dithiophene-2,6-diyl][3-fluoro-2-[(2-ethylhexyl)carbonyl]thieno[3,4-b]thiophenediyl]] (PTB7) as the electron donor and [6,6]-phenyl-C71butyric acid methyl ester ($PC_{71}BM$) as the electron acceptor. The PTB7:$PC_{71}BM$ active blending layer (~80 nm) was prepared by spin-coating a mixed solvent of chlorobenzene/1,8-diiodoctane (97:3% by volume) solution (concentration, 25 mg mL^{-1}) at 800 rpm for 1 min. The device was then pumped down under vacuum (<10^{-6} Torr), and MoO_3 (5 nm) and Ag (100 nm) electrodes were then deposited. The area of the Ag electrode defines the active area of the device as 13.0 mm^2. PCE values were determined from *J–V* curve measurements (using IviumStat source meter, Ivium Technologies, Eindhoven, The Netherlands) under a 1 sun, AM 1.5G spectrum from a solar simulator (Portable Solar Simulator PEC-L01, Peccell Technologies Inc., Kanagawa, Japan; 1000 W m^{-2}).

Solar cell characterization: EQE measurements were obtained by using the PV Measurements system, applying monochromatic light from a xenon lamp under ambient conditions. The details are given in the literature.[43] The impedance spectra were measured using electrical impedance spectroscopy (SI 1287 from Solartron Analytical) and the oscillation amplitude of the AC voltage was maintained at 10 mV for all impedance measurements.[14]

The absorption of real devices of ITO/ZnO-R/PTB7:$PC_{71}BM$/MoO_3/Ag with and without 2-ME+EA treatment were determined by values based on the reflection mode (Fig. S2, Supporting Information). The details are given in the literature.[44]

Supporting Information

Supporting Information is available from the Wiley Online Library or from the authors.

Acknowledgements

This work was supported by Korea Institute of Materials Science (KIMS) and the National Research Foundation of Korea (NRF) grant (No. 2012R1A2A2A06046931, 2009-0093020) by the Ministry of Science, ICT & Future Planning (MSIP), Korea. This work was also supported by the Future Strategic Fund (1.130061.01) of UNIST(Ulsan National Institute of Science and Technology) and KIST-UNIST Ulsan Center (KUUC) for Convergent Materials and Low Dimensional Carbon Materials. The portion of this research conducted at the University of Ulsan was supported by Priority Research Centers Program through the National Research Foundation of Korea (NRF) funded by the Ministry of Education (2009–0093818).

Received: July 1, 2013
Published online:

[1] G. Yu, J. Gao, J. C. Hummelen, F. Wudl, A. J. Heeger, *Science* **1995**, *270*, 1789.
[2] B. C. Thompson, J. M. J. Fréchet, *Angew. Chem. Int. Ed.* **2008**, *47*, 58.
[3] S. H. Park, A. Roy, S. Beaupre, S. Cho, N. Coates, J. S. Moon, D. Moses, M. Leclerc, K. Lee, A. J. Heeger, *Nat. Photonics* **2009**, *3*, 297.
[4] P. W. M. Blom, V. D. Mihailetchi, L. J. A. Koster, D. E. Markov, *Adv. Mater.* **2007**, *19*, 1551.
[5] H. L. Yip, A. K. Y. Jen, *Energy Environ. Sci.* **2012**, *5*, 5994.
[6] G. Li, R. Zhu, Y. Yang, *Nat. Photonics* **2012**, *6*, 153.
[7] Z. C. He, C. M. Zhong, S. J. Su, M. Xu, H. B. Wu, Y. Cao, *Nat. Photonics* **2012**, *6*, 591.

© 2013 WILEY-VCH Verlag GmbH & Co. KGaA, Weinheim

[8] Y. J. Cheng, S. H. Yang, C. S. Hsu, *Chem. Rev.* **2009**, *109*, 5868.
[9] Y. Y. Liang, Z. Xu, J. B. Xia, S. T. Tsai, Y. Wu, G. Li, C. Ray, L. P. Yu, *Adv. Mater.* **2010**, *22*, E135.
[10] J. Peet, J. Y. Kim, N. E. Coates, W. L. Ma, D. Moses, A. J. Heeger, G. C. Bazan, *Nat. Mater.* **2007**, *6*, 497.
[11] H. Y. Chen, J. H. Hou, S. Q. Zhang, Y. Y. Liang, G. W. Yang, Y. Yang, L. P. Yu, Y. Wu, G. Li, *Nat. Photonics* **2009**, *3*, 649.
[12] J. Y. Kim, K. Lee, N. E. Coates, D. Moses, T. Q. Nguyen, M. Dante, A. J. Heeger, *Science* **2007**, *317*, 222.
[13] Z. C. He, C. Zhang, X. F. Xu, L. J. Zhang, L. Huang, J. W. Chen, H. B. Wu, Y. Cao, *Adv. Mater.* **2011**, *23*, 3086.
[14] H. Choi, J. S. Park, E. Jeong, G. H. Kim, B. R. Lee, S. O. Kim, M. H. Song, H. Y. Woo, J. Y. Kim, *Adv. Mater.* **2011**, *23*, 2759.
[15] Y. H. Zhou, C. Fuentes-Hernandez, J. Shim, J. Meyer, A. J. Giordano, H. Li, P. Winget, T. Papadopoulos, H. Cheun, J. Kim, M. Fenoll, A. Dindar, W. Haske, E. Najafabadi, T. M. Khan, H. Sojoudi, S. Barlow, S. Graham, J.-L. Brédas, S. R. Marder, A. Kahn, B. Kippelen, *Science* **2012**, *336*, 327.
[16] H. Kang, S. Hong, J. Lee, K. Lee, *Adv. Mater.* **2012**, *24*, 3005.
[17] C. E. Small, S. Chen, J. Subbiah, C. M. Amb, S. W. Tsang, T. H. Lai, J. R. Reynolds, F. So, *Nat. Photonics* **2012**, *6*, 115.
[18] K. Lee, J. Y. Kim, S. H. Park, S. H. Kim, S. Cho, A. J. Heeger, *Adv. Mater.* **2007**, *19*, 2445.
[19] L. M. Chen, Z. Xu, Z. R. Hong, Y. Yang, *J. Mater. Chem.* **2010**, *20*, 2575.
[20] J. Y. Kim, S. H. Kim, H. H. Lee, K. Lee, W. L. Ma, X. Gong, A. J. Heeger, *Adv. Mater.* **2006**, *18*, 572.
[21] Y. M. Sun, C. J. Takacs, S. R. Cowan, J. H. Seo, X. Gong, A. Roy, A. J. Heeger, *Adv. Mater.* **2011**, *23*, 2226.
[22] A. K. K. Kyaw, X. W. Sun, C. Y. Jiang, G. Q. Lo, D. W. Zhao, D. L. Kwong, *Appl. Phys. Lett.* **2008**, *93*, 221107.
[23] C. Y. Li, T. C. Wen, T. H. Lee, T. F. Guo, J. C. A. Huang, Y. C. Lin, Y. J. Hsu, *J. Mater. Chem.* **2009**, *19*, 1643.
[24] M. Campoy-Quiles, T. Ferenczi, T. Agostinelli, P. G. Etchegoin, Y. Kim, T. D. Anthopoulos, P. N. Stavrinou, D. D. C. Bradley, J. Nelson, *Nat. Mater.* **2008**, *7*, 158.
[25] Z. Xu, L. M. Chen, G. W. Yang, C. H. Huang, J. H. Hou, Y. Wu, G. Li, C. S. Hsu, Y. Yang, *Adv. Funct. Mater.* **2009**, *19*, 1227.
[26] D. Kabra, L. P. Lu, M. H. Song, H. J. Snaith, R. H. Friend, *Adv. Mater.* **2010**, *22*, 3194.
[27] H. Ma, H. L. Yip, F. Huang, A. K. Y. Jen, *Adv. Funct. Mater.* **2010**, *20*, 1371.
[28] B. R. Lee, H. Choi, J. SunPark, H. J. Lee, S. O. Kim, J. Y. Kim, M. H. Song, *J. Mater. Chem.* **2011**, *21*, 2051.
[29] J. H. Seo, A. Gutacker, Y. M. Sun, H. B. Wu, F. Huang, Y. Cao, U. Scherf, A. J. Heeger, G. C. Bazan, *J. Am. Chem. Soc.* **2011**, *133*, 8416.
[30] Z. C. He, C. M. Zhong, X. Huang, W. Y. Wong, H. B. Wu, L. W. Chen, S. J. Su, Y. Cao, *Adv. Mater.* **2011**, *23*, 4636.
[31] T. B. Yang, M. Wang, C. H. Duan, X. W. Hu, L. Huang, J. B. Peng, F. Huang, X. Gong, *Energy Environ. Sci.* **2012**, *5*, 8208.
[32] X. F. Liu, W. Wen, G. C. Bazan, *Adv. Mater.* **2012**, *24*, 4505.
[33] H. Zhou, Y. Zhang, J. Seifter, S. D. Collins, C. Luo, G. C. Bazan, T.-Q. Nguyen, A. J. Heeger, *Adv. Mater.* **2013**, *25*, 1646.
[34] N. Sekine, C. H. Chou, W. L. Kwan, Y. Yang, *Org. Electron.* **2009**, *10*, 1473.
[35] C. Goh, S. R. Scully, M. D. McGehee, *J. Appl. Phys.* **2007**, *101*, 114503.
[36] H. Choi, H. Cho, S. Song, H. Suh, S. Park, J. Y. Kim, *Phys. Chem. Chem. Phys.* **2010**, *12*, 15309.
[37] G. Jayalakshmi, N. Gopalakrishnan, T. Balasubramanian, *J. Alloys Compd.* **2013**, *551*, 667.
[38] T. M. Barnes, J. Leaf, S. Hand, C. Fry, C. A. Wolden, *J. Appl. Phys.* **2004**, *96*, 7036.
[39] H. Mali, I. Sakaguchi, N. Ohashi, S. Sekiguchi, H. Haneda, J. Tanaka, N. Ichinose, *Jpn. J. Appl. Phys.* **2003**, *42*, 75.
[40] D. C. Lim, K. D. Kim, S. Y. Park, E. M. Hong, H. O. Seo, J. H. Lim, K. H. Lee, Y. Jeong, C. Song, E. Lee, Y. D. Kim, S. Cho, *Energy Environ. Sci.* **2012**, *5*, 9803.
[41] D. C. Lim, W. H. Shim, K. D. Kim, H. O. Seo, J. H. Lim, Y. Jeong, Y. D. Kim, K. H. Lee, *Sol. Energy Mater. Sol. Cells* **2011**, *95*, 3036.
[42] J. H. Chu, J. Kwak, T. Y. Kwon, S. D. Park, H. Go, S. Y. Kim, K. Park, S. Kang, S. Y. Kwon, *ACS Appl. Mater. Interfaces* **2012**, *4*, 1777.
[43] M. Heo, H. Cho, J. W. Jung, J. R. Jeong, S. Park, J. Y. Kim, *Adv. Mater.* **2011**, *23*, 5689.
[44] M.-H. Chen, J. Hou, Z. Hong, Z. Hong, G. Yang, S. Sista, L. M. Chen, Y. Yang, *Adv. Mater.* **2009**, *21*, 4238.

© 2013 WILEY-VCH Verlag GmbH & Co. KGaA, Weinheim